Dalton Transactions

ROYAL SOCIETY OF CHEMISTRY

PAPER

View Article Online
View Journal

Check for updates

Cite this: DOI: 10.1039/d1dt03334d

Monitoring spin-crossover phenomena *via* Re(I) luminescence in hybrid Fe(II) silica coated nanoparticles†

Ismael Francisco Díaz-Ortega,[a,b] Eva Luz Fernández-Barbosa,[a] Silvia Titos-Padilla,[a] Simon J. A. Pope,[c] Juan-Ramón Jiménez,*[a] Enrique Colacio *[a] and Juan Manuel Herrera *[a]

Received 1st October 2021,
Accepted 22nd October 2021

DOI: 10.1039/d1dt03334d

rsc.li/dalton

Bare (**1**) and silica coated (**1@SiO$_2$**) spin crossover (SCO) nanoparticles based on the polymer {[Fe(NH$_2$Trz)$_3$](BF$_4$)$_2$}$_n$ have been prepared following a water-in-oil synthetic procedure. For **1**, the critical temperatures of the spin transition are $T_C\downarrow$ = 214.6 K and $T_C\uparrow$ = 220.9 K. For **1@SiO$_2$**, the abruptness of the transition is enhanced and the critical temperatures are centred at room temperature ($T_C\downarrow$ = 292.1 K and $T_C\uparrow$ = 296.3 K). An inert Re(I) complex of formula [Re(phen)(CO)$_3$(PETES)](PF$_6$) (phen = 1, 10-phenanthroline; PETES = 2(4-pyridylethyl)triethoxysilane) (**Re**) was also synthesized yielding intense green emission centred at λ_{em} = 560 nm. The grafting of this complex on the silica shell of **1@SiO$_2$** led to a bifunctional SCO-luminescence composite (**1@SiO$_2$/Re**) whose luminescence properties were tuned by the spin state switching. Temperature-variable photophysical studies showed that luminescence and spin transition were synchronized through a radiative (trivial) energy transfer mechanism between the Re(I) and the Fe(II)-LS (LS, Low Spin) centres.

Introduction

In the last few years, many efforts have been devoted to the preparations of bifunctional nanomaterials combining spin crossover (SCO) behaviour and luminescence properties.[1–4] These systems, in which the thermally induced spin transition tunes the luminescence signal are interesting from a fundamental point of view, and also for potential applications such as the development of photonic devices and thermal sensors. Indeed, in certain conditions, the detection of changes in the emission intensity can be preferable and more sensitive to the variation of the optical or magnetic properties of the material. Piguet *et al.* pave the way to prepare luminescence SCO compounds in the early 2000s. They synthesized a series of heterodimetallic SCO Fe(II)–Eu(III) complexes where the lanthanide emission was partially obscured through an intramolecular Eu(III) → Fe(II)-HS (High Spin) Förster energy transfer or quantitatively quenched due to spectral overlap between Eu(III)-based emission and Fe(II)-LS (Low Spin) absorptions.[5–7] Since then, a significant number of compounds showing synergy between both properties have been reported. Most of these systems are based on Fe(II) SCO complexes and green-emitting luminophores. In the LS regime, the spectral overlap between the emission and the metal-to-ligand charge transfer (MLCT) and/or spin-allowed d–d ($^1A_1 \rightarrow {}^1T_1$, $^1A_1 \rightarrow {}^1T_2$) absorptions of the Fe(II) centres, causes the luminescence quenching. When the LS → HS transition is thermally induced, weaker MLCT bands are found and the d–d transitions move to the near infrared region (*ca.* 900 nm), the emitter–acceptor spectral overlap vanish and the emission intensity increases. In order to combine the luminophore and the SCO moiety in the same material, two different approaches have mainly been considered. The first of them combines the SCO active moiety and the emitter in a single coordination compound. The emitter can be an organic fluorophore or luminescent complex which acts as: (i) ligand towards the Fe(II) centres;[8–17] (ii) counterion;[18] or (iii) guest molecules inserted within the cavities of three-dimensional SCO frameworks.[19,20] In these cases, the location of both components can be studied through structural elucidation techniques allowing the accurate determination of the nature of the correlation between the SCO and the lumine-

[a]Departamento de Química Inorgánica, Facultad de Ciencias, Universidad de Granada and Unidad de Excelencia de Química (UEQ), Avda. Fuentenueva s/n, 18071 Granada, Spain. E-mail: jmherrera@ugr.es
[b]Departamento de Química y Física-CIESOL, Universidad de Almería, Ctra. Sacramento s/n, 04120, Almería
[c]Cardiff School of Chemistry, Cardiff University, Cardiff, CF10 3AT, UK

† Electronic supplementary information (ESI) available: X-ray powder diffraction diagrams, elemental analyses, ^{1}H-NMR spectrum of **Re**, additional photophysical experiments (reflectance spectra, excited state decay profiles and excitation spectra measured at different temperatures) and magnetic properties of **1@SiO$_2$/Re**. See DOI: 10.1039/d1dt03334d

Open Access Article. Published on 25 October 2021. Downloaded on 11/8/2021 12:00:44 PM.
This article is licensed under a Creative Commons Attribution-NonCommercial 3.0 Unported Licence.

Open Access Article. Published on 25 October 2021. Downloaded on 11/8/2021 12:00:44 PM.
This article is licensed under a Creative Commons Attribution-NonCommercial 3.0 Unported Licence.

scence phenomena. A second strategy deals with the synthesis of SCO composites doped or decorated with luminescence species.[21–25] In these cases, the location of both components is uncertain and to determine the interaction mechanism is challenging. However, as both units are almost chemically independent, it is possible to use different luminophores or modify their chemical nature without affecting significantly to the magnetic and optical properties of the SCO moiety. For example, Bousseksou and co-workers prepared a set of nanoparticles based on the Fe(II)-triazole family of coordination polymers doped with different organic fluorophores. Depending on the fluorophore nature, the emission was more or less efficiently modulated by the spin transition which remained almost identical compared to the non-doped material.[21,22] Following a more elaborated strategy, our group prepared core SCO nanoparticles based on the $\{[Fe(HTrz)_2(Trz)](BF_4)\}_n$ polymer (Trz = 1,2,4-1*H*-triazole) embedded within a silica shell. In these hybrid Fe-Trz@SiO_2 nanoparticles, the magnetic and optical bistability of the Fe(II) polymer was preserved. Dansyl fluorophores were covalently attached to their surface through alcoxysilane groups. In the low spin regime, the dansyl centered emission was quenched due to its spectral overlap with the absorption bands of the Fe(II) centres.[23,24] However, due to the low thermal stability of the dansyl fluorophore, the emissive signal is progressively lost upon successive heating–cooling cycles. The use of more robust luminophores, such as Tb(III) complexes, allowed to confirm that the thermal variation of the emission was invariably synchronized with the SCO over several successive thermal cycles.[25]

Thus, to avoid decomposition of the emissive moieties, the use of robust luminescence complexes seems a wise strategy. Another strategy deals with a decrease of the critical temperatures at which the spin transition takes place. For the Fe-triazole family of polymers, it is well known that the nature of the 4-substituent on the triazole ligand tunes the cooperativity and the spin transition over a wide range of temperatures.[26] For example, compared to the polymers based on the 1,2,4-triazole ligand, the 4-substituted 4-amino-1,2,4-triazole (NH_2-Trz) analogues show lower critical temperatures and narrower thermal hysteresis loops of *ca.* 10 K wide.[27,28] In this work, both possibilities have been considered. First, we have prepared bare and silica coated nanoparticles based on the $\{[Fe(NH_2\text{-}Trz)_3](BF_4)_2\}_n$ polymer. Then, the surface of the SiO_2 coated nanoparticles has been decorated with a robust green-emitting Re(I) complex. The structural, magnetic and optical properties of these new materials are presented.

Experimental section

Materials and chemicals

Solvents and the reactants 1,10-phenanthroline (phen), 2(4-pyridylethyl)triethoxysilane (PETES), tetraethyl orthosilicate (TEOS), rhenium pentacarbonyl chloride, 4-amino-1,2,4-triazole and iron(II) tetrafluoroborate were obtained from commercial sources and used as received.

Instrumentation and characterization

Nanoparticles were characterized by transmission electron microscopy (TEM) using a LIBRA 120 PLUS Carl Zeiss electron microscope operating at 200 keV. 5 mg of the material was redispersed by sonication (30 min) in 1 mL of EtOH. Carbon reinforced copper grids (200 mesh) were submerged into suspension 50 times and then allowed to dry in air for at least 48 h. The size of the particles was determined by "manual counting" using ScionImage software (http://www.scioncorp.com). HAADF-STEM images and EDX analyses were recorded on a HAADF FEI TITAN G2 instrument working at an accelerating voltage of 200 kV in the scanning mode with a probe diameter of 0.5 nm. Elemental analyses were carried out on a Fisons-Carlo Erba analyser model EA 1108. Magnetic measurements were obtained with the use of a Quantum Design SQUID magnetometer MPMS-XL operating at a magnetic field of 10 000 G in the 100–350 K temperature range. The heating–cooling cycles were performed with a rate of 10 K min^{-1}. X-Ray powder diffraction data (Cu Kα, λ = 1.5418 Å) were collected at 25 °C on a Bruker D8 Discover vertical scan diffractometer equipped with a PILATUS3R 100K-A detector. The generator was operated at 50 kV and 1 mA. The powders were gently ground in an agate mortar and then deposited in the hollow of an aluminium holder equipped with a zero-background plate. The diffractograms were collected in the range of 2θ between 6°–55° at steps of 0.02° during 30 seconds per step. NMR characterizations were carried out on a 400 MHz (2 channels) BRUKER Nanobay Advance III. Reflectance spectra were recorded on a Varian Cary 5 UV-vis-NIR spectrophotometer equipped with a specially designed Praying Mantis diffuse reflection attachment. Emission and excitation spectra were measured on a UV-VIS-PTI QuantaMaster™ 8000 spectrofluorometer equipped with a Picosecond Photon Detector (230–850 nm, PPD-850, HORIBA Scientific) and a continuous Xenon Short Arc Lamp (190–2000 nm, USHIO). The temperature-ramp measurements (270 K–330 K) were recorded using an optical Closed Cycle Cryocooler (ARS DE-202PE) adapted for solid samples (45° angle with respect to the incoming excitation source). All the spectra (emission and excitation) were corrected with Real-time corrections function. TCSPC lifetime measurements were performed using a 375 nm excitation wavelength provided by a pulsed diode light source NanoLED 375L (<200 ps pulse, HORIBA Scientific).

All these techniques are available at the Centro de Instrumentación Científica (CIC) of the University of Granada.

Syntheses

Synthesis of $\{[Fe(NH_2\text{-}Trz)_3](BF_4)_2\}_n$ nanoparticles (1). These nanoparticles were prepared following the synthetic procedure described previously by our research group.[23] Briefly, 1 mmol of $Fe(BF_4)_2{\cdot}6H_2O$ (337 mg) were dissolved in 0.5 mL of deionized water and added to a mixture of Triton X-100 (1.8 mL), *n*-hexanol (1.8 mL) and cyclohexane (7.5 mL) and stirred until formation of a clear water-in-oil microemulsion. A similar procedure was applied to prepare a microemulsion of 4-amino-

This journal is © The Royal Society of Chemistry 2021

Open Access Article. Published on 25 October 2021. Downloaded on 11/8/2021 12:00:44 PM.
This article is licensed under a Creative Commons Attribution-NonCommercial 3.0 Unported Licence.

1,2,4-triazole (NH_2-Trz) (252 mg, 3 mmol in 0.5 mL of deionized H_2O). Both microemulsions were quickly combined and the mixture stirred vigorously for 24 h. After this time, acetone was added to break the microemulsion. The precipitated nanoparticles were recovered by centrifugation, washed several times with EtOH, acetone and finally dried at 50 °C for 12 h.

Synthesis of hybrid {[Fe(NH_2-Trz)$_3$][BF_4)$_2$}@SiO_2 nanoparticles (1@SiO_2). These nanoparticles were prepared as **1** but adding 0.1 mL of tetraethyl orthosilicate (TEOS) to the microemulsions containing the Fe(II) and NH_2-Trz reactants before they were mixed.

Synthesis of the Re(I) complex [Re(phen)(CO)$_3$(PETES)](PF$_6$) (Re). In a first step, the intermediate complex [Re(phen)(CO)$_3$(CH_3CN)](PF_6) was prepared. 0.5 g of $Re(CO)_5Cl$ (1.4 mmol) and the equimolar amount of 1,10-phenanthroline (phen) (250 mg) were suspended in 30 mL of toluene and the mixture was stirred at reflux for 16 h under a N_2 atmosphere. After this time a yellow precipitate was formed. The reaction was cold down to room temperature and the precipitate filtered, washed with toluene and dried under vacuum. The product was re-suspended in 50 mL of CH_3CN and 1 equiv. of $AgPF_6$ was added. The mixture was heated to reflux for 12 h in the dark and the formed AgCl filtered off. The resulting yellow solution was reduced to dryness, re-dissolved in a minimal amount of CH_3CN and diethyl ether was added to precipitate the desired intermediate complex as a yellow powder. Next, 0.1 g of this intermediate (0.157 mmol) and 1.2 molar equiv. of 2(4-pyridilethyl)triethoxysilane (PETES) were added to 20 mL of CH_2Cl_2 and the mixture heated to reflux for 5 h. The resulting solution was evaporated to dryness, re-dissolved in a minimal amount of CH_2Cl_2 and Et_2O was added to precipitate the [Re(phen)(CO)$_3$(PETES)](PF$_6$) (**Re**) conjugate as a yellow-orange powder. Yield = 68%. ^{1}H NMR (CD_3Cl, δ ppm): 9.53 (d, 2H), 8.79 (d, 2H), 8.22–8.16 (m, 4H), 8.05 (d, 2H), 7.10 (d, 2 H), 3.27–3.18 (m, 6 H), 2.58–2.54 (dd, 2 H), 1.09 (t, 9 H), 0.83–0.69 (dd, 2H). ESI-MS (*m*/*z*, positive mode): 718.15 $(M - PF_6)^+$. Elem. Anal. Found (calcd for $C_{28}H_{34}N_3O_6PF_6ReSi$): C, 38.57 (38.75); H, (4.08 (3.95); N 4.91 (4.84).

Surface functionalization of 1@SiO_2 with the luminescent rhenium complex Re (1@SiO_2/Re). 0.1 g of **1@SiO_2** were suspended in a solution containing 0.1 g of **Re** dissolved in 40 mL of a mixture CH_2Cl_2/EtOH (1/1, v/v) and heated to reflux for 60 h. After this time, the nanoparticles were recovered by centrifugation and washed successively with acetonitrile, ethanol and acetone until the luminescence signal of the rhenium complex was not observed in the washings' solvents. Finally, **1@SiO_2/Re** was dried at 50 °C for 16 hours.

Results and discussion

Synthesis and structural characterization of SCO nanoparticles 1 and 1@SiO_2

Based on a classical water-in-oil synthetic approach, bare [Fe(NH_2Trz)$_3$](BF_4)$_2$ (**1**) and core/shell [Fe(NH_2Trz)$_3$](BF_4)$_2$@SiO_2 (**1@SiO_2**) nanoparticles were prepared following the procedure described previously by our research group.[23] Two microemulsions containing Fe(BF_4)$_2$·6H_2O or 4-amino-1,2,4-triazole (NH_2Trz) ligand and appropriate amounts of surfactants, co-surfactants, an oil phase a (for **1@SiO_2** the silica precursor tetraethylorthosilicate, TEOS, was additionally added to both microemulsions), were prepared separately and then mixed and stirred vigorously for 24 h at room temperature. After this time, acetone was added to the colourless microemulsion causing the nanoparticles precipitation. In the case of **1@SiO_2**, a change of colour to deep violet was observed. This colour change, associated with the HS → LS transition in the Fe-NH_2Trz polymer, demonstrates that such a transition takes place at room-temperature and can be induced by small stimuli, such as for example, a change in the polarity of the solvent around the Fe(II) polymer. The white colour of **1** did not change after the addition of acetone, which indicates that in this case, the HS → LS transition takes place at lower temperatures. HR-TEM images of **1** and **1@SiO_2** are shown in Fig. 1. In both cases the nanoparticles display a long and thin rod-like shape. For **1**, the width of the nanoparticles is regular with a mean value of 35.28 ± 5.95 nm. Conversely, the length is quite heterogeneous, with sizes that vary between 100 nm and 650 nm. Statistically, the calculated mean length is 288.70 ± 133.12 nm. **1@SiO_2** nanoparticles show a homogeneous mean length of 317.9 ± 75.0 nm and a mean width of 45.3 ± 7.3 nm. In both cases, the nanoparticles are monodisperse and well defined.

The X-ray powder diffraction patterns of both samples match well with that shown by the bulk Fe-NH_2-Trz polymer (Fig. S1†). A lower degree of crystallinity is observed for **1@SiO_2**, which is attributed to the amorphous nature of the silica shell. The elemental analyses (Table S1†) reveal the analogy between these two samples and the bulk material. For **1@SiO_2**, an estimated molar ratio Fe/SiO_2 of 1/1.5 was found.

Synthesis and photophysical characterization of [Re(phen)(CO)$_3$(PETES)]PF$_6$ (Re)

The Re-alcoxysilane conjugate [Re(phen)(CO)$_3$(PETES)]PF_6 (**Re**) was obtained following the synthetic procedure depicted in Scheme 1a. In a first step, the reaction of equimolar amounts of $Re(CO)_5Cl$ and 1,10-phenanthroline in toluene afforded the well-known complex [Re(phen)(CO)$_3$Cl].[29] Further reaction with $AgPF_6$ in CH_3CN gave the cationic complex [Re(phen)(CO)$_3$(CH_3CN)]PF_6, which is highly soluble in common organic solvents. The coordinated acetonitrile molecule can be easily displaced by others ligands such as pyridine derivates.[30] Reaction of this complex with the alcoxysilane derivate 2(4-pyridilethyl)triethoxysilane (PETES) provided the desired Re-alcoxysilane conjugate **Re** in a very good yield and with a high degree of purity (Fig. S2†).

The absorption and emission spectra of this complex recorded in CH_2Cl_2 solutions are shown in Fig. 2a. The absorption spectrum shows two main peaks at 220 nm and 274 nm which correspond to the $\pi \leftarrow \pi^*$ transitions of the PETES and 1,10-phenanthroline respectively. A band of lower intensity located at 365 nm corresponds to the π^*(phen) ← dπ(Re)

Open Access Article. Published on 25 October 2021. Downloaded on 11/8/2021 12:00:44 PM.
This article is licensed under a Creative Commons Attribution-NonCommercial 3.0 Unported Licence.

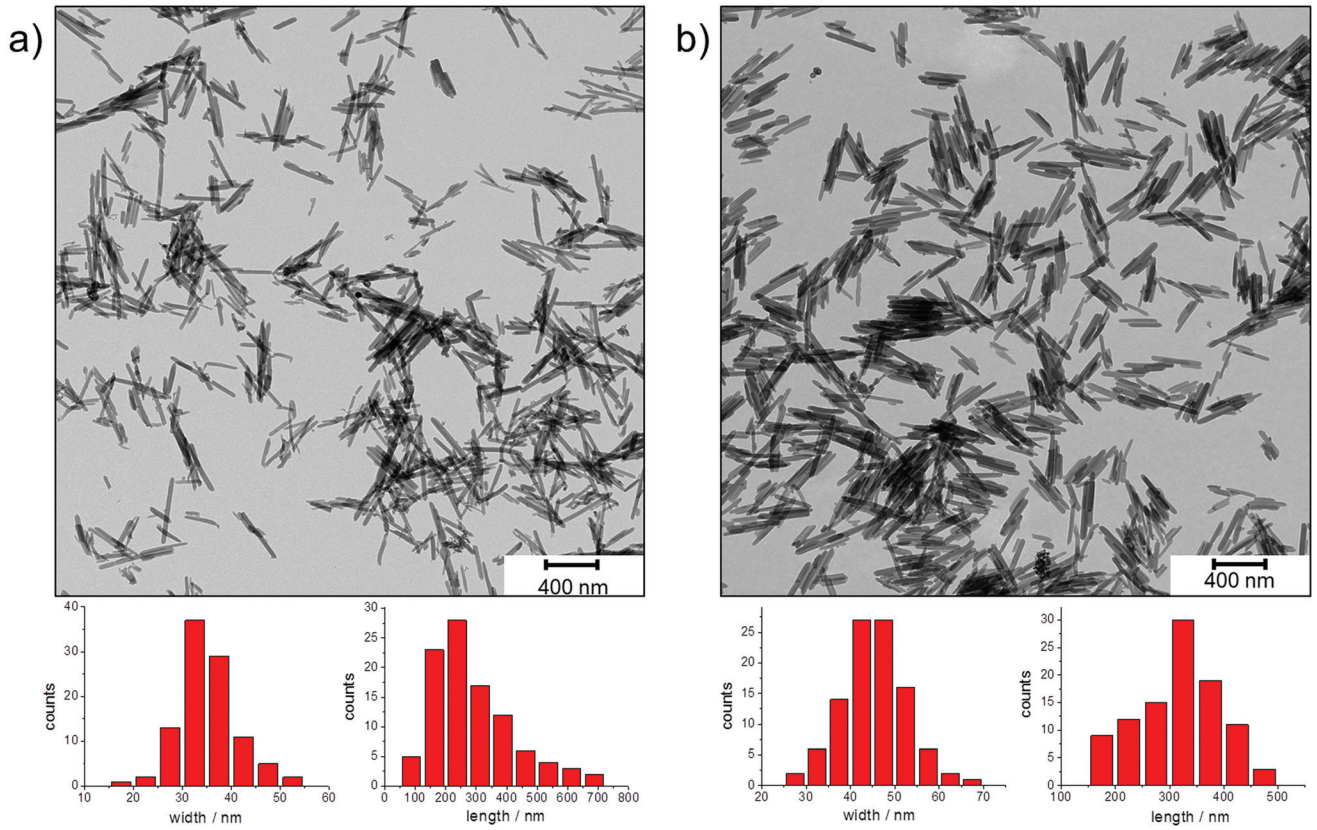

Fig. 1 HR-TEM images and size distribution histograms of samples **1** (a) and **1@SiO$_2$** (b).

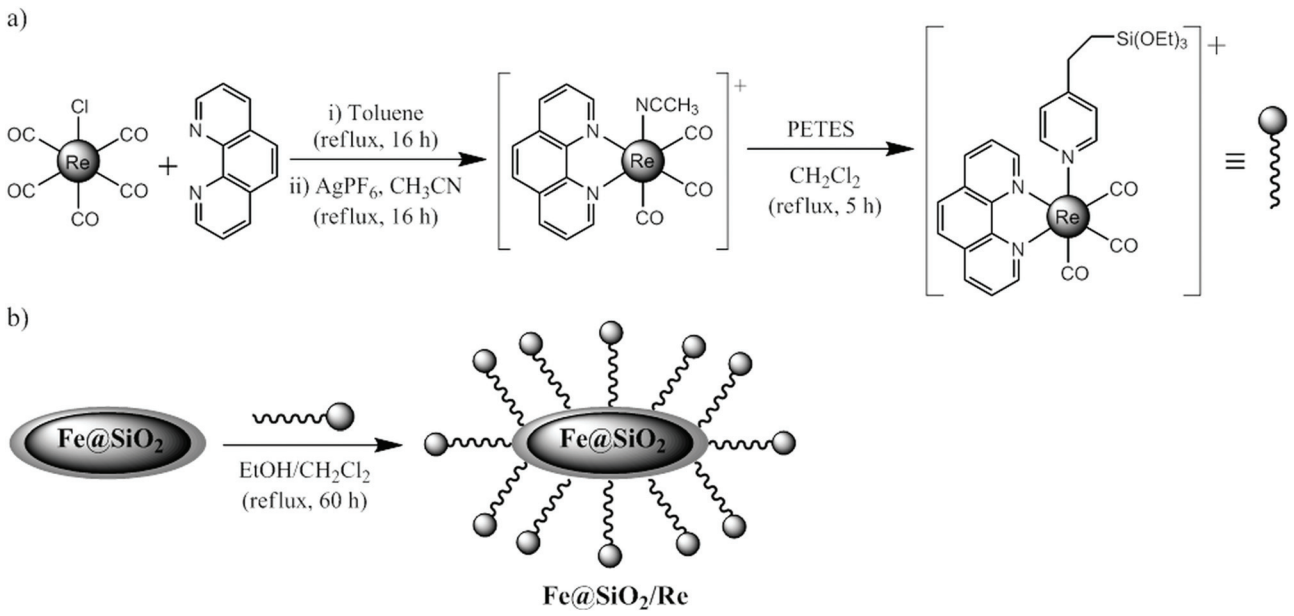

Scheme 1 Syntheses of the Re-alcoxisilane conjugate [Re(phen)(CO)$_3$(PETES)]PF$_6$ (**Re**) (a) and the hybrid nanoparticles **1@SiO$_2$/Re** (b).

^{1}MLCT transition. Excitation at 365 nm yields an intense and unstructured emission band centred at 560 nm. This emission band is ascribed to the radiative deexcitation from a ^{3}MLCT level. In the solid state, the emission is slightly blue shifted due to rigidochromic effect, with the maximum located at 525 nm. To establish the dependence of the emission with the temperature, solid state emission spectra were recorded between 275 K and 330 K (Fig. 2b). A small decrease of the

 This journal is © The Royal Society of Chemistry 2021

Open Access Article. Published on 25 October 2021. Downloaded on 11/8/2021 12:00:44 PM.
This article is licensed under a Creative Commons Attribution-NonCommercial 3.0 Unported Licence.

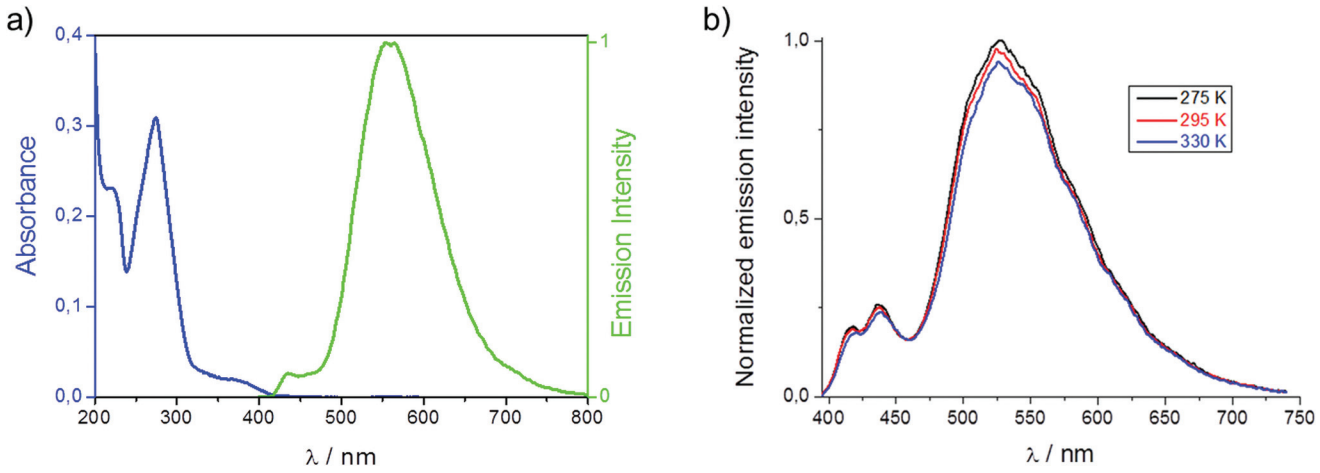

Fig. 2 (a) Room temperature UV-Vis (blue) and emission (green) spectra of complex **Re** in dichloromethane. (b) Solid state emission spectra of complex **Re** measured in the temperature range 275 K–330 K.

emission intensity of *ca.* 5% is observed. This behaviour indicates that the thermal quenching of the **Re** luminescence is not significant in this range of temperature.

Solid-state emission lifetime measurements were performed at T = 273 K and 330 K and the kinetic decay fitted to a double-exponential (Fig. S4†). The mean excited-state lifetimes show a decrease by a factor of 0.82 (2875 ns at 273 K and 2346 ns at 330 K) upon increasing the temperature (Table S2†).

This new heteroleptic **Re** complex can be easily embedded and/or grafted to the surface of silica nanoparticles. At the best of our knowledge, no examples of hybrid Re(I)-silica nanoparticles have been previously reported.

Synthesis and structural characterization of bifunctional SCO/luminescence nanoparticles 1@SiO_2/Re

To functionalize the surface of **1@SiO_2** with the **Re** conjugate, both species were suspended in a mixture of CH_2Cl_2/EtOH (1 : 1, v/v) and stirred at reflux for 60 h (Scheme 1b). After several washing steps to remove unreacted species, hybrid **1@SiO_2/Re** nanoparticles were isolated as a pale yellow powder. HAADF-STEM and EDX-compositional mapping images are shown in Fig. 3. The images confirm that the Re(I) complex is grafted to the silica shell and randomly distributed across the whole surface of the nanoparticle. A mean atomic Fe/Re ratio of 20/1 was found. Elemental analysis (Table S1†) did not provide a precise formula for this sample, due to the complexity of the material and the fact that the **Re** complex is randomly distributed on the nanoparticles (it can be attached on their surface through the total or partial hydrolysis of the three ethoxy groups). Nevertheless, the increase in the C and H percentages found compared to **1@SiO_2** indicates the effective graft of the **Re** complex onto the nanoparticles.

Magnetic properties

The magnetic properties of **1** and **1@SiO_2** in the form of $\chi_M T$ *vs.* T are represented in Fig. 4. For **1**, the $\chi_M T$ value at 350 K is

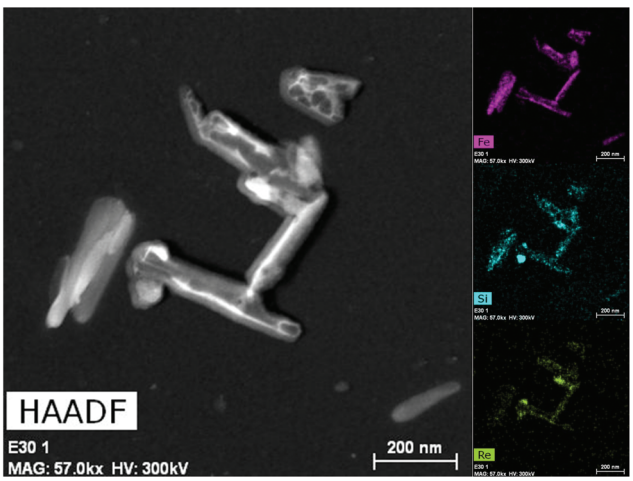

Fig. 3 HAADF-STEM image (left) and EDX compositional maps (left) of Fe, Si and Re (top, middle and bottom respectively) of sample **1@SiO_2 : Re**.

equal to 3.49 cm^3 K mol^{-1}, close to the expected value for an high spin Fe(II) ion. Upon cooling, the $\chi_M T$ product decreases sharply at $T_C\downarrow$ = 214.6 K to reach a value of 0.257 cm^3 K mol^{-1} at 100 K, which indicates that approximately 7.4% of the Fe(II) centres remain in HS configuration at this temperature. On the warming cycle, the LS → HS transition takes place at $T_C\uparrow$ = 220.9 K, thus displaying a thermal hysteresis loop of 6.3 K wide. Compared to the bulk sample,[26] the critical temperatures of the spin transition in **1** decrease noticeably about 30 K and the hysteresis loop slightly narrows. This behaviour is usually observed when the size of the particles decreases from the micro- to the nanoscale.[31–34] For **1@SiO_2** the spin transition moves to higher temperatures and appears centred at room temperature ($T_C\downarrow$ = 292.1 K, $T_C\uparrow$ = 296.3 K, ΔT_C = 4.2 K). To quantify the abruptness of the transition, the ΔT_{80} parameter was determined (Table 1).[35] This parameter corresponds

Open Access Article. Published on 25 October 2021. Downloaded on 11/8/2021 12:00:44 PM.
This article is licensed under a Creative Commons Attribution-NonCommercial 3.0 Unported Licence.

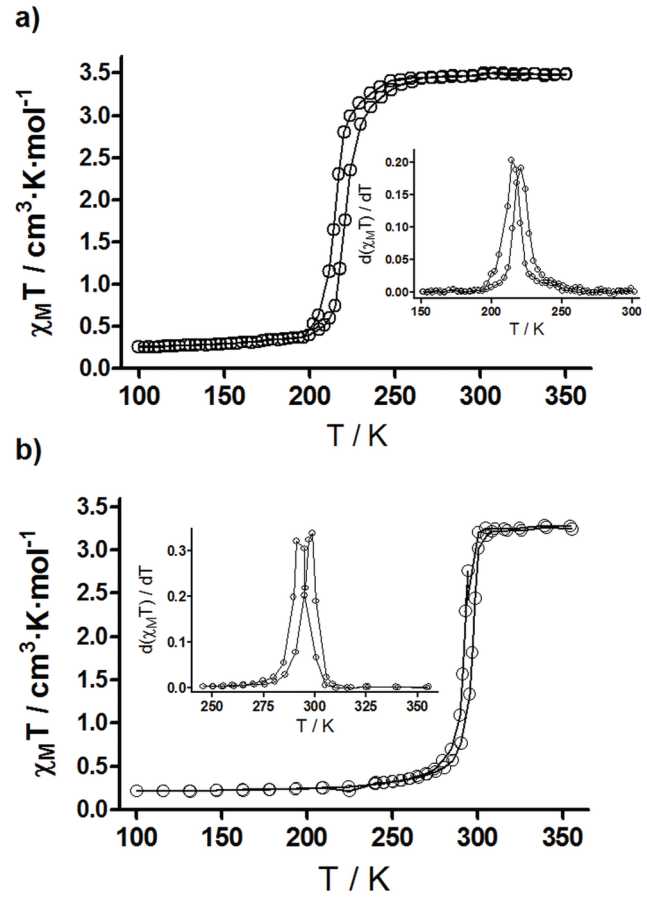

Fig. 4 Thermal variation of the $\chi_M T$ products for samples **1** (a) and **1@SiO$_2$** (b).

Table 1 Physical parameters characteristics of the spin transition for samples **1**, **1@SiO$_2$** and **1@SiO$_2$/Re**

	$T_C\downarrow$[a] (K)	$\Delta T_{80}\downarrow$	$T_C\uparrow$[a] (K)	$\Delta T_{80}\uparrow$	ΔT (K)	% $HS_{150\ K}$[b]
1	214.6	13.1	220.9	13.6	6.3	8.4
1@SiO$_2$	292.1	19.1	296.3	19.4	4.2	6.8
1@SiO$_2$/Re	290.2	20.1	297.3	20.2	7.1	10.3

[a] $T_C\downarrow$ and $T_C\uparrow$ are the critical temperature for the HS–LS and LS–HS transitions in the cooling and warming modes respectively. [b] $\%HS_{150\ K}$ represents the percentage of residual Fe(II) ions that remain in the HS state below $T_C\downarrow$.

to the difference of temperatures at which 80% and 20% of the Fe(II) ions switch their electronic configuration. When the nanostructured Fe(II) polymer is embedded within a silica shell, the transition is more abrupt as indicated by a higher ΔT_{80} parameter (Table 1). The changes observed in the physical parameters of the LS ↔ HS transition for **1** and **1@SiO$_2$** are due to the well-known effects that the rigid silica matrix embedding the nanoparticles exerts on the magnetic properties of these materials.[36–39] Finally, for **1@SiO$_2$/Re**, the thermal variation of $\chi_M T$ is quite similar to **1@SiO$_2$** (Fig. S6† and Table 1) revealing that the LS ↔ HS transition is barely affected by the surface functionalization of the silica nanoparticles.

Thermal dependence of the luminescence properties of 1@SiO$_2$/Re

To determine if the emission properties of the rhenium complex are correlated with the spin transition of the Fe(II) centres in **1@SiO$_2$/Re**, variable-temperature emission spectra have been recorded in the range between 290 K and 340 K. As shown in Fig. 5a, at 290 K the emission is almost identical to the isolated **Re** complex. As the temperature rises (heating cycle), the emission intensity grows continuously to reach a 2.2-fold increase at 340 K. When the temperature falls back to 290 K (cooling cycle), the intensity of the emission also decreases gradually up to 290 K, with both spectra at this temperature, before and after the thermal cycle, being virtually identical. The thermal variation of the luminescence intensity for the heating/cooling cycle (Fig. 5b) describes a hysteresis cycle 8 K wide ($T_C\uparrow$ = 323 K and $T_C\downarrow$ = 315 K), very similar to that observed for the thermal variation of the magnetic properties (Fig. S6†). Although a deviation of *ca.* 20 K exists between the critical temperatures for the thermal variation of the $\chi_M T$ product ($T_C\uparrow$ = 290 K and $T_C\downarrow$ = 297 K) and the luminescence, which is probably due to instrumental limitations (emissive and magnetic experiments were carried out at different temperature-sweep speeds), it is evident that emission intensity and SCO transition are synchronized. To determine the thermal stability of the rhenium complex in this system, the sample was exposed to successive heating/cooling cycles between 290 K and 340 K (Fig. 5c). After five cycles, the emissions at high and low temperature are alike, confirming the stability of the rhenium complex in this range of temperature. Additionally, variable-temperature excitation spectra were also recorded (Fig. S7†). A broad excitation band centred at λ = 389 nm is observed whose intensity increases as the temperature rises, reaching a maximum at 340 K and returning to the initial value when the temperature drops back to 280 K (cooling cycle). The thermal variation of the excitation and emission intensity maxima display identical hysteresis cycles (Fig. 5d and b respectively). These experiments demonstrate that changes in the Re(I) emission intensity and thermally induced spin transition in the Fe(II) centres are synchronized.

These results constitute a new example of bifunctional SCO-Luminescent system where the emission properties of the luminophore are regulated by the electronic configuration of the Fe(II) centres through an energy transfer mechanism. Full spectral overlap between the **Re** ^{3}MLCT emission and d–d absorption bands of the Fe(II)-LS ions exists (Fig. S3†), which is a necessary condition for energy transfer (ET) to occur. To elucidate the nature of the energy transfer, it is necessary to determine if the emission lifetime of the Re(I) moieties are affected by the spin transition. For a radiative (trivial) ET process, donor and acceptor are independent and the photons emitted by the Re(I) complex are simply reabsorbed by the Fe(II)-LS centres. In this case, the emission lifetime of the luminophore remains unchanged, regardless of the electronic configuration

This journal is © The Royal Society of Chemistry 2021

Open Access Article. Published on 25 October 2021. Downloaded on 11/8/2021 12:00:44 PM.
This article is licensed under a Creative Commons Attribution-NonCommercial 3.0 Unported Licence.

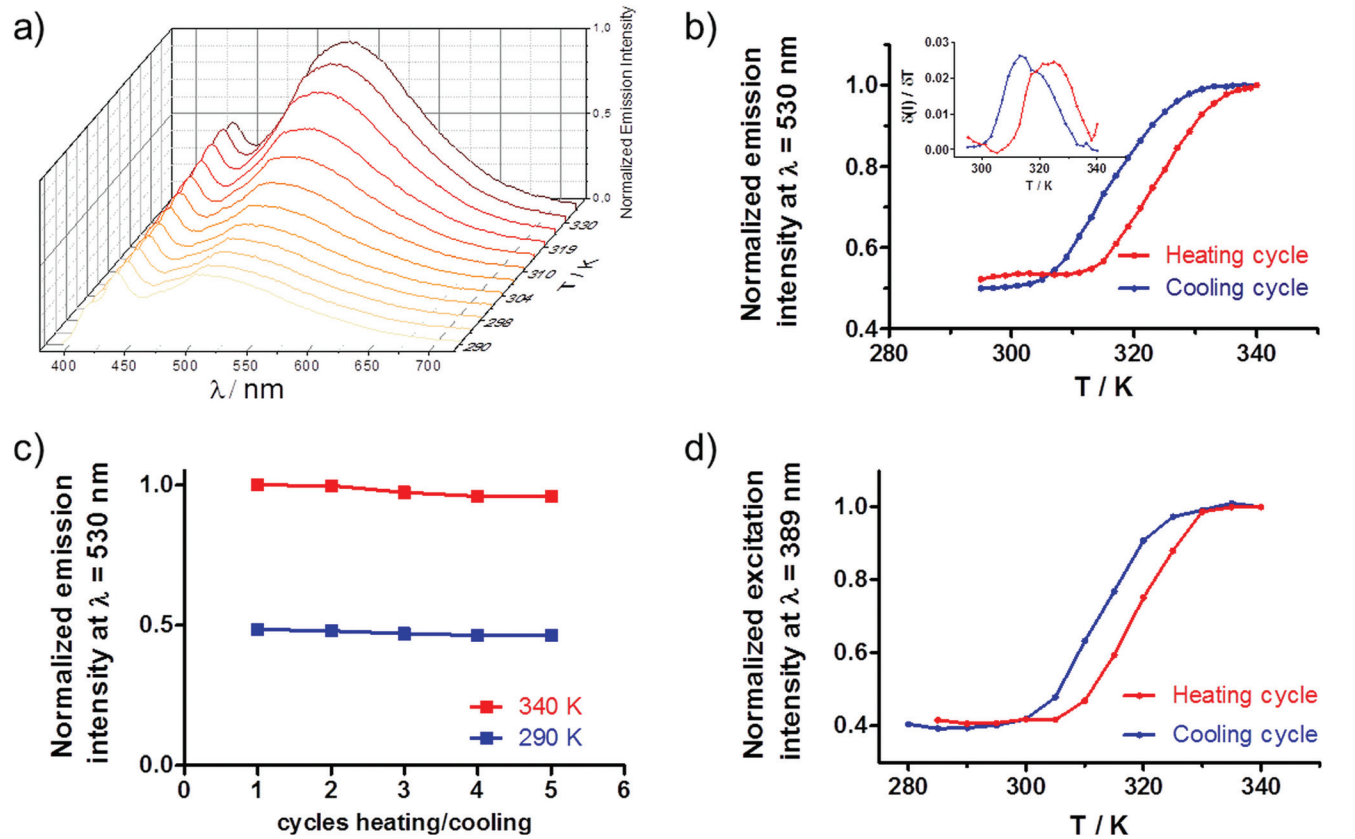

Fig. 5 For sample **1@SiO$_2$/Re**. (a) Gradual increase of the emission intensity as the temperature increases from 290 K to 340 K (λ_{exc} = 365 nm). (b) Thermal variation of the emission intensity at λ_{em} = 530 nm for two successive heating (red) and cooling (blue) cycles between 294 K and 340 K. (c) Emission intensity at λ_{em} = 530 nm for five successive heating/cooling cycles at 330 K and 273 K. (d) Thermal variation of the excitation intensity at λ = 389 nm for two successive heating (red) and cooling (blue) cycles between 294 K and 340 K.

of the Fe(II) ions. Conversely, for a non-radiative Förster resonance energy transfer (FRET), the emission lifetime in the presence of acceptor Fe(II)-LS ions will decrease according to the efficiency of the process, as the presence of acceptors constitutes an additional pathway for the deactivation of the emitter's excited state. Solid state lifetime measurements were performed at 273 K and 323 K (Fig. S5†). The kinetic decays were fitted to a three-exponential function which indicates the existence of different chemical environments around the Re(I) centres (Table S2†). The average lifetimes found were 39 ns (T = 273 K) and 33 ns (T = 330 K), which represents a decrease of the emission lifetime by a factor of *ca.* 0.84. For the free **Re** complex the average lifetimes were significantly longer (see above), which suggest the existence of dynamic quenching between the Re(I) and the Fe(II) moieties. However, the decrease in the lifetime induced by the rise of temperature in **Re** was about 18%, *i.e.* a factor of 0.82, quite similar to that observed for **1@SiO$_2$/Re**. Thus, the decrease of the emission lifetimes observed in **1@SiO$_2$/Re** between 273 K and 330 K is mainly due to the rise of temperature and/or instrumental error and independent of the Fe(II) spin state. These results suggest that trivial energy transfer occurs between the Re complex and the SCO compound and rules out the existence of significant FRET.

Conclusions

In summary, bare and silica coated nanocomposites have been prepared based on the SCO Fe(II) polymer $\{[Fe(NH_2Trz)_3](BF_4)_2\}_n$ and characterized from a structural and magnetic point of view. Compared to the bulk, bare Fe-NH$_2$Trz nanoparticles exhibit a spin transition with a similar cooperativity, although the critical temperatures of the transition decrease significantly. The cooperativity increases when the nanoparticles are embedded within a silica shell as well as the critical temperatures which appear in this case centred at room temperature.

A robust luminescent Re(I) complex was grafted onto the silica shell of the nanoparticles affording a bifunctional SCO-luminescence material highly stable towards photo-bleaching and temperature. Temperature-variable photo-physical studies revealed that emissive properties and Fe(II) spin state are synchronized. In the LS regime, the Re(I)-based ^{3}MLCT emission is obscured due to the existence of a radiative Re(I) → Fe(II)-LS energy transfer where the emitted photons are reabsorbed by the d–d absorption bands of the Fe(II)-LS centres. The viability of 5d^6 luminescence complexes to prepare highly stable bifunctional SCO-luminescence materials has been demonstrated.

Open Access Article. Published on 25 October 2021. Downloaded on 11/8/2021 12:00:44 PM.
This article is licensed under a Creative Commons Attribution-NonCommercial 3.0 Unported Licence.

Conflicts of interest

There are no conflicts to declare.

Acknowledgements

Financial support from Projects CTQ2014-56312-P and PGC2018-102052-B-C21 financed by MCIN/AEI/10.13039/501100011033/FEDER "Una manera de hacer Europa", the Junta de Andalucía (FQM-195), Feder project A-FQM-172-UGR18 and the University of Granada is gratefully acknowledged. I.-F. Díaz-Ortega and J.-R Jiménez are also thankful to the Junta de Andalucía for Postdoctoral research fellowships.

References

1 C. M. Quintero, G. Félix, I. Suleimanov, J. S. Costa, G. Molnár, L. Salmon, W. Nicolazzi and A. Bousseksou, *Beilstein J. Nanotechnol.*, 2014, **5**, 2230–2239.
2 H. J. Shepherd, C. M. Quintero, G. Molnár, L. Salmon and A. Bousseksou, in *Spin-Crossover Materials: Properties and Applications*, John Wiley & Sons Ltd, Oxford, UK, 2013, pp. 347–373.
3 K. Senthil Kumar and M. Ruben, *Coord. Chem. Rev.*, 2017, **346**, 176–205.
4 H. J. Shepherd, G. Molnár, W. Nicolazzi, L. Salmon and A. Bousseksou, *Eur. J. Inorg. Chem.*, 2013, **2013**, 653–661.
5 C. Edder, C. Piguet, G. Bernardinelli, J. Mareda, C. G. Bochet, J. C. G. Bunzli and G. Hopfgartner, *Inorg. Chem.*, 2000, **39**, 5059–5073.
6 C. Edder, C. Piguet, J. C. G. Bünzli and G. Hopfgartner, *Chem. – Eur. J.*, 2001, **7**, 3014–3024.
7 T. Lathion, A. Fürstenberg, C. Besnard, A. Hauser, A. Bousseksou and C. Piguet, *Inorg. Chem.*, 2020, **59**, 1091–1103.
8 M. Hasegawa, F. Renz, T. Hara, Y. Kikuchi, Y. Fukuda, J. Okubo, T. Hoshi and W. Linert, *Chem. Phys.*, 2002, **277**, 21–30.
9 Y. Garcia, F. Robert, A. D. Naik, G. Zhou, B. Tinant, K. Robeyns, S. Michotte and L. Piraux, *J. Am. Chem. Soc.*, 2011, **133**, 15850–15853.
10 C. F. Wang, G. Y. Yang, Z. S. Yao and J. Tao, *Chem. – Eur. J.*, 2018, **24**, 3218–3224.
11 J. L. Wang, Q. Liu, Y. S. Meng, X. Liu, H. Zheng, Q. Shi, C. Y. Duan and T. Liu, *Chem. Sci.*, 2018, **9**, 2892–2897.
12 C. Lochenie, K. Schötz, F. Panzer, H. Kurz, B. Maier, F. Puchtler, S. Agarwal, A. Köhler and B. Weber, *J. Am. Chem. Soc.*, 2018, **140**, 700–709.
13 J. Yuan, S. Q. Wu, M. J. Liu, O. Sato and H. Z. Kou, *J. Am. Chem. Soc.*, 2018, **140**, 9426–9433.
14 B. Benaicha, K. Van Do, A. Yangui, N. Pittala, A. Lusson, M. Sy, G. Bouchez, H. Fourati, C. J. Gómez-Garciá, S. Triki and K. Boukheddaden, *Chem. Sci.*, 2019, **10**, 6791–6798.
15 J. Y. Ge, Z. Chen, L. Zhang, X. Liang, J. Su, M. Kurmoo and J. L. Zuo, *Angew. Chem., Int. Ed.*, 2019, **58**, 8789–8793.
16 S. Ghosh, S. Kamilya, T. Pramanik, M. Rouzières, R. Herchel, S. Mehta and A. Mondal, *Inorg. Chem.*, 2020, **59**, 13009–13013.
17 B. Schäfer, T. Bauer, I. Faus, J. A. Wolny, F. Dahms, O. Fuhr, S. Lebedkin, H. C. Wille, K. Schlage, K. Chevalier, F. Rupp, R. Diller, V. Schünemann, M. M. Kappes and M. Ruben, *Dalton Trans.*, 2017, **46**, 2289–2302.
18 H. Matsukizono, K. Kuroiwa and N. Kimizuka, *Chem. Lett.*, 2008, **37**, 446–447.
19 T. Delgado, M. Meneses-Sánchez, L. Piñeiro-López, C. Bartual-Murgui, M. C. Muñoz and J. A. Real, *Chem. Sci.*, 2018, **9**, 8446–8452.
20 M. Meneses-Sánchez, L. Piñeiro-López, T. Delgado, C. Bartual-Murgui, M. C. Muñoz, P. Chakraborty and J. A. Real, *J. Mater. Chem. C*, 2020, **8**, 1623–1633.
21 L. Salmon, G. Molnár, D. Zitouni, C. Quintero, C. Bergaud, J. C. Micheau and A. Bousseksou, *J. Mater. Chem.*, 2010, **20**, 5499–5503.
22 C. M. Quintero, I. A. Gural'Skiy, L. Salmon, G. Molnár, C. Bergaud and A. Bousseksou, *J. Mater. Chem.*, 2012, **22**, 3745–3751.
23 S. Titos-Padilla, J. M. Herrera, X.-W. Chen, J. J. Delgado and E. Colacio, *Angew. Chem., Int. Ed.*, 2011, **50**, 3290–3293.
24 J. M. Herrera, S. Titos, S. Pope, I. Berlanga, F. Zamora, J. J. Delgado, K. Kamenev, X. Wang, A. Prescimone, E. K. Brechin and E. Colacio, *J. Mater. Chem. C*, 2015, 7819–7829.
25 I. Suleimanov, O. Kraieva, G. Molnár, L. Salmon and A. Bousseksou, *Chem. Commun.*, 2015, **51**, 15098–15101.
26 O. Roubeau, *Chem. – Eur. J.*, 2012, **18**, 15230–15244.
27 M. B. Bushuev, L. G. Lavrenova, V. N. Ikorskii, Y. G. Shvedenkov, V. A. Varnek, L. A. Sheludyakova and S. V. Larionov, *Russ. J. Coord. Chem. Khim.*, 2004, **30**, 284–290.
28 V. A. Varnek and L. G. Lavrenova, *J. Struct. Chem.*, 1995, **36**, 104–111.
29 M. Wrighton and D. L. Morse, *J. Am. Chem. Soc.*, 1974, **96**, 998–1003.
30 *Photochemistry and Photophysics of Coordination Compounds II*, ed. V. Balzani and S. Campagna, Springer Berlin Heidelberg, Berlin, Heidelberg, 2007, vol. 281.
31 I. Boldog, A. B. Gaspar, V. Martínez, P. Pardo-Ibañez, V. Ksenofontov, A. Bhattacharjee, P. Gütlich and J. A. Real, *Angew. Chem., Int. Ed.*, 2008, **47**, 6433–6437.
32 T. Forestier, S. Mornet, N. Daro, T. Nishihara, S. I. Mouri, K. Tanaka, O. Fouché, E. Freysz and J. F. Létard, *Chem. Commun.*, 2008, 4327–4329.
33 T. Forestier, A. Kaiba, S. Pechev, D. Denux, P. Guionneau, C. Etrillard, N. Daro, E. Freysz and J. F. Létard, *Chem. – Eur. J.*, 2009, **15**, 6122–6130.
34 F. Volatron, L. Catala, E. Rivière, A. Gloter, O. Stéphan and T. Mallah, *Inorg. Chem.*, 2008, **47**, 6584–6586.
35 K. Jonas, A. Jean-Paul, C. Renée, C. Epiphane, K. Olivier, J. G. Haasnoot, G. Françoise, J. Charlotte, A. Bousseksou,

 This journal is © The Royal Society of Chemistry 2021

Open Access Article. Published on 25 October 2021. Downloaded on 11/8/2021 12:00:44 PM.
This article is licensed under a Creative Commons Attribution-NonCommercial 3.0 Unported Licence.

L. Jorge, V. François and G. V. Anne, *Chem. Mater.*, 1994, **6**, 1404–1412.

36 G. Chastanet, C. a. Tovee, G. Hyett, M. a. Halcrow and J.-F. Létard, *Dalton Trans.*, 2012, **41**, 4896–4902.

37 M. P. Cuéllar, A. Lapresta-Fernández, J. M. Herrera, A. Salinas-Castillo, M. D. C. Pegalajar, S. Titos-Padilla, E. Colacio and L. F. Capitán-Vallvey, *Sens. Actuators, B*, 2015, **208**, 180–187.

38 A. Lapresta-Fernández, M. P. Cuéllar, J. M. Herrera, A. Salinas-Castillo, M. D. C. Pegalajar, S. Titos-Padilla, E. Colacio and L. F. Capitán-Vallvey, *J. Mater. Chem. C*, 2014, **2**, 7292–7303.

39 P. Durand, S. Pillet, E. E. Bendeif, C. Carteret, M. Bouazaoui, H. El Hamzaoui, B. Capoen, L. Salmon, S. Hébert, J. Ghanbaja, L. Aranda and D. Schaniel, *J. Mater. Chem. C*, 2013, **1**, 1933–1942.